CHAPTER

5 Combining serial block face and focused ion beam scanning electron microscopy for 3D studies of rare events

Christopher J. Guérin[a,b,c], Anna Kremer[a,b,c], Peter Borghgraef[a,b,c], Andy Y. Shih[d,e], Saskia Lippens[a,b,c,*]

[a]*VIB BioImaging Core, VIB, Ghent, Belgium*

[b]*VIB Inflammation Research Center, VIB, Ghent, Belgium*

[c]*Department of Biomedical Molecular Biology, Ghent University, Ghent, Belgium*

[d]*Seattle Children's Research Institute, Center for Developmental Biology and Regenerative Medicine, Seattle, WA, United States*

[e]*Department of Pediatrics, University of Washington, Seattle, WA, United States*

**Corresponding author: e-mail address: saskia.lippens@irc.vib-ugent.be*

Chapter outline

Methods in Cell Biology, Volume 152, ISSN 0091-679X, https://doi.org/10.1016/bs.mcb.2019.03.014

Abstract

Volume electron microscopy allows for the automated acquisition of serial-section imaging data that can be reconstructed in three-dimensions (3D) to provide a detailed, geometrically accurate view of cellular ultrastructure. Two, volume electron microscopy (EM) techniques, serial block face scanning electron microscopy (SBF-SEM) and focused ion beam scanning electron microscopy (FIB-SEM), use a similar slice-and-view approach but differ in their fields of view and 3D resolution. This chapter highlights a workflow where the ability of SBF-SEM to image a large field of view is combined with the precise sectioning capability of FIB-SEM to first locate a rare cellular event in a large tissue volume and then inspect the event with higher resolution. Using these two EM platforms in synergy is a powerful technique and can be useful for both simple structural studies as well as correlative studies using both light and electron microscopy.

1 Introduction

For many of the 80+ years since electron microscopy was introduced, it was a largely two-dimensional (2D) technique. Transmission electron microscopy (TEM) images through very thin sections of plastic embedded tissues, with the thickness of the sample determined by the accelerating voltage of the microscope. Penetration of the electron beam is limited to roughly 1 nm/kV. TEM tomography, where a section is imaged through a series of tilt angles and then reconstructed using a back projection or an inverse Fourier transform algorithm does give a 3D result, but is limited in volume (Koster et al., 1997). Scanning electron microscopy (SEM) can image 3D surface features but only yields a 2D projection of the surface with minimal sub-surface information.

With the introduction of SBF-SEM (Denk & Horstmann, 2004; Leighton, 1981) and FIB-SEM (Heymann et al., 2006), larger volumes of cells and tissues were accessible to 3D ultrastructural analysis (Peddie & Collinson, 2014). Both techniques use SEM to image the surface of a sample embedded in plastic resin, and both slice off a portion of that surface between images. The major difference between the techniques is the thickness of the surface removed, and thus the interval between the sections in the Z (or axial) dimension. Another important difference is the field of view (FOV) of the different techniques. SBF-SEM has a larger FOV, at correspondingly low magnification, but FOVs of hundreds of microns are possible. The sample size is limited by the width of the diamond knife and the mechanics of the microtome that is used for sectioning it. In a commercial version, marketed by Gatan

under the name 3View, samples are limited to a maximum of 1 × 1 × 1 mm, and a typical minimum voxel size is X, Y, Z = 5 × 5 × 50 nm. FIB-SEMs differ in their capabilities depending on the specifications of the ion and electron columns, but some are able to image samples at isotropic voxel dimensions of 5 nm. Their FOV though is more limited and imaging volumes will typically not exceed 30 × 15 × 20 nm.

Brain pericytes are closely associated with the endothelium of blood vessels and contribute to the formation and maintenance of the blood brain barrier (BBB) (Daneman, Zhou, Kebede, & Arres, 2010), as well as regulation of cerebral blood flow (Hall et al., 2014). Their far-reaching processes do not cover the entire cell basement membrane of the vascular endothelia, and their cell bodies occur only intermittently along capillaries (Hartmann et al., 2015). During stroke, pericytes are thought to constrict around the vessels, possibly exacerbating reperfusion, and then detach from the vessels mediating inflammation and secondary neuronal death following the acute phase (Yang et al., 2017). Finding these cells during TEM requires some luck, as their presence cannot be assured in every section. Furthermore, their interactions with the underlying vascular endothelium can be extensive and a single TEM image does not reveal their complex 3D structure.

Volume EM has the potential to reveal the full extent of pericyte structure and can also show their physical interaction with glia, neurons, and other vascular cell types. To image the fine subcellular structures of pericytes in 3D requires FIB-SEM, but locating sporadic pericytes within a limited FOV is difficult. Pericytes in the brain frequently occur at capillary branch points so locating an area where two vessels may be about to come together provides a way to target the FIB to a ROI that has a high likelihood of containing a pericyte. Using the large FOV of the SBF-SEM and its ability to search in 3D within a tissue sample, it is possible to locate vessels that are coming to a branch point. Once these have been identified, the same sample can be moved between the SBF-SEM and the FIB to allow the pericyte to be imaged at high resolution. This chapter will describe our workflow for imaging of pericytes but is equally applicable to other sporadic or rare tissue structures.

2 Methods

2.1 Tissue preparation, fixation and staining

Wild type mice were administered an overdose of anesthetic to produce an insensate state and their thoracic cavity was opened to reveal the heart. A fine cannula was introduced into the left ventricle and isotonic saline pH 7.2 containing 20 units/mL of heparin at 37 °C was infused into the vascular system at a pressure just below normal mouse mean arterial blood pressure (100 mmHg). A small opening was made in the right atrium to provide outflow and saline perfusion carried on for 2 min or until the draining fluids were mostly clear. The perfusion fluid was then switched to a modified Karnovsky fixation solution containing 2% paraformaldehyde and 2% gluteraldehyde with 20 mM $CaCl_2$ in 0.2 M Na cacodylate

buffer pH 7.2 at 37 °C. Perfusion was continued for 12 min (NB perfusion pressure should not exceed normal mouse blood pressure, approx. 100 mm Hg). At the end of the perfusion the skull was removed and the brain excised. Cubes of 1 mm of primary sensory cortex were isolated by dissection and placed in the same fixative mixture overnight at 4 °C.

The following day, tissues were post-fixed using a variation of the protocol from the NCMIR (Deerinck, Bushong, Thor, & Ellisman, 2010) In brief, the blocks of tissue were incubated for 1 h on an orbital shaker in OsO_4 reduced with potassium ferricyanide, washed, and then incubated in thiocarbohydrazide, repeated by OsO_4, TCH and OsO_4 again. Tissues were further stained en bloc with Uranyl Acetate, then lead citrate, and dehydrated using microwave assisted processing as shown in detail in Table 1. The samples were further dehydrated through two, 5 min steps of propylene oxide, to remove any residual water then transferred to a mixture of 50% propylene oxide and 50% Spurr's Epoxy resin then placed on a rotator and the mixture was allowed to infiltrate the tissue overnight at room temperature. The next day samples were transferred to 100% Spurr's Epoxy and rotated for a further 2 h then transferred to fresh 100% resin in beem capsules and placed in an oven set to 60 °C for 48–36 h to polymerize and harden.

2.2 Trimming and mounting

Once the resin blocks were hardened, they were removed from the oven and the tissue was isolated from excess resin and trimmed to a pyramid shape using a razor blade. The pyramid was then mounted on a metal pin using conductive epoxy resin (NB to improve conductivity and prevent charging in the SEM it is critical that the underside of the tissue makes contact with the metal pin so any excess resin must be removed before mounting). The block face and sides of the pyramid were smoothed using an ultramicrotome and a diamond knife. Finally, the sample was coated with 2–5 nm of platinum using a sputter coater to further enhance conductivity.

2.3 Imaging in the SBF-SEM

The sample on the pin was placed into the carrier that fits into the 3View ultramicrotome. Using a binocular dissecting microscope placed on the SEM door containing the 3View, the sample was brought to a distance of 0.1–0.5 mm from the diamond knife. The lateral position of the knife and the beginning of the cutting window are adjusted as necessary. Using the 3View controls in Gatan digital micrograph software the sample was approached and the surface is smoothed with the 3View knife. The chamber door was then closed and the system placed under vacuum. The block face was imaged (usually with an accelerating voltage in the range of 1.5–2 kV), and an area where two capillaries are in the same ROI is found by alternatively taking an image then removing a small number $(1-10)$ of 70 nm sections with the 3View knife. When a likely area was found further imaging and sectioning was carried out to ensure the vessels appear to be moving into close proximity indicating the likelihood of a branch point just below the block face. At this point the sample was removed from the SBF-SEM.

Table 1 Protocol for microwave processing.

Program #	Description	User prompt (on/off)	Time (hr:min:sec)	Power (Watts)	Temp (°C)	Load Cooler (off/auto/on)	Vacuum/Bubbler pump (off/bubb/vac cycle/vac on/vap)	Steady temp	
								Pump (on/off)	temp (°C)
8	TCH	Off	0:01:00	150	50	Off	Vacuum cycle	On	30
		Off	0:01:00	0	50	Off	Vacuum cycle	On	30
		Off	0:01:00	150	50	Off	Vacuum cycle	On	30
15	0.1 M Cacodylate	On	0:00:40	250	50	Off	Vacuum cycle	On	30
	0.1 M Cacodylate	On	0:00:40	250	50	Off	Vacuum cycle	On	30
9	Osmium	Off	0:02:00	100	50	Off	Vacuum cycle	On	30
		Off	0:02:00	0	50	Off	Vacuum cycle	On	30
		Off	0:02:00	100	50	Off	Vacuum cycle	On	30
		Off	0:02:00	0	50	Off	Vacuum cycle	On	30
		Off	0:02:00	100	50	Off	Vacuum cycle	On	30
16	Uranyl acetate	OFF	0:01:00	150	50	Off	Vacuum cycle	On	30
		Off	0:01:00	0	50	Off	Vacuum cycle	On	30
		Off	0:01:00	150	50	Off	Vacuum cycle	On	30
		Off	0:01:00	0	50	Off	Vacuum cycle	On	30
		Off	0:01:00	150	50	Off	Vacuum cycle	On	30
		Off	0:01:00	0	50	Off	Vacuum cycle	On	30
		Off	0:01:00	150	50	Off	Vacuum cycle	On	30
15	ddH_2O	On	0:00:40	250	50	Off	Vacuum cycle	On	30
	ddH_2O	On	0:00:40	250	50	Off	Vacuum cycle	On	30
10	50% EtOH	On	0:00:40	150	50	Off	Off	On	30
	70% EtOH	On	0:00:40	150	50	Off	Off	On	30
	90% EtOH	On	0:00:40	150	50	Off	Off	On	30
	100% EtOH	On	0:00:40	150	50	Off	Off	On	30
	100% EtOH	On	0:00:40	150	50	Off	Off	On	30

2.4 Imaging in the FIB-SEM

The sample still mounted on its pin was coated with a layer of ≈20 nm platinum using a sputter coater and placed into the FIB-SEM sample carrier. This was placed into vacuum in the SEM chamber and while imaging at 15 kV (to see through the platinum coating), the ROI identified in the SBF-SEM is re-located. Next, the carrier was moved into the concentric point of the FIB and SEM beam. The ROI was reacquired based on the morphological features seen in the SBF-SEM. The following steps are done under the control of ATLAS 3D software. A further protective platinum layer was deposited over the imaging area using gas injection and the FIB beam, on top of which tracking marks are milled to allow autofocus, stigmation correction and tracking during sectioning. Next, these tracking marks are protected by depositing a layer of carbon using gas-injection and the FIB beam. The ROI was prepared for imaging by using the Ga^+-ion beam to remove material from in front of the block face so the e-beam can image it. An imaging window was defined and then the software will automatically collect a stack of images. Accelerating electron beam voltages for imaging are typically in the 1–2 kV range.

2.5 Registering images and creating a stack

The images were loaded into ImageJ/Fiji and aligned using the SIFT plugin. (NB If it is necessary to reduce the size of the data stack for easy manipulation, the pixel data can be binned by adjusting the image size.) Brightness and contrast can be adjusted and the data saved as a .tif format stack.

2.6 Segmenting out structures of interest

In order to visualize specific structures of interest, it is necessary to segment these out of the dataset by determining which pixels belong to the structure of interest, as opposed to "background." This part of the process requires a significant amount of manual input, even if semi-automated solutions are used. Different software packages can be used to achieve this, such as Fiji with TrackEM2 plugin, Microscopy Image Browser (MIB) (Belevich, Joensuu, Kumar, Vihinen, & Jokitalo, 2016), SuRVos (Darrow et al., 2017), and others. Here, we used MIB with the Brush-tool to create the pericyte model, by drawing over its cell membrane. The model was exported as a 3D-TIF.

2.7 Rendering the segmented structures

For rendering of the data we made use of Imaris by importing the image stacks containing the EM recordings and the segmented pericyte as different channels. We created an object of the pericyte in which the visualization can be customized in terms of color and transparency. The final 3D view on the full cellular structure can then be rendered. Orthogonal slicing of the volume with the EM data, allows examination of the dataset in any of the x–y, y–z or x–z orientations.

3 Materials and instrumentation

3.1 Tissue preparation, fixation and staining

Instrumentation

Perfusion apparatus (in house, see Supplemental Fig. 1 in the online version at https://doi.org/10.1016/bs.mcb.2019.03.014)
Vacuum oven (LabLine, ThermoFisher)
Rotator (13916-824, VWR)
Orbital shaker (PSMBD, Grant Bio)

Materials

0.2 M Cacodylate (sodium) buffer pH 7.4 (11652, EMS)
10% paraformaldehyde (15712, EMS)
25% gluteraldehyde (G-5882, Sigma)
Calcium Chloride (223506, Sigma-Aldrich)
Karnovsky fixative: 2% paraformaldehyde, 2.5% gluteraldehyde in 0.1 M cacodylate buffer pH 7.4
Reduced Osmium: 1 part 4% OsO4 (19150, EMS) + 1 part 3% potassium ferricyanide (EMS 20150) in 0.2 M cacodylate pH 7.4
1% Thiocarbohydrazide: dissolve 0.1 g TCH (21900, EMS) in UPW. Incubate 1 h in an oven at 60 °C. Shake every 10′
Osmium (19150, EMS)
Uranyl acetate (22400 EMS)
Walton's Lead Aspartate staining solution: Prepare L-Aspartic acid solution by dissolving 0.998 g L-Aspartic acid (A8949, Sigma) in 250 mL UPW. Adjust to pH 3.8 with 1 N KOH. Dissolve 0.066 g Lead Nitrate (07905CJ, Sigma-Aldrich) in 10 mL L-Aspartic acid (A8949, Sigma-Aldrich) pH 3.8. Adjust to pH 5.5 with 1 N KOH. Check pH with pH indicator strip (109584.1111, Millipore)
Ethanol (1.00983, Merck)
Propylene oxide (82320, Sigma)
Durcupan (44610, Sigma)
Spurr's resin (14300, EMS)
Low-melt agarose (A4018, Sigma)
beem capsules (69910-01, EMS)

3.2 Trimming and mounting

Instrumentation

Ultramicrotome (Ultracut, Riechert-Jung-NB no longer available)
Sputter Coater (Q150T ES, Quorum)
Diamond knife (40-HIS, Diatome Histo knife)

Materials

Aluminium pin (Gatan)
Conductive epoxy (496-265, Circuit works, RS Components)

3.3 Imaging in the SBF-SEM

Instrumentation

Merlin SEM (Zeiss) with 3View (Gatan) and Focal Charge Compensator (Zeiss)

3.4 Imaging in the FIB-SEM

Crossbeam 540 (Zeiss) with ATLAS software (FIBICS)

3.5 Registering images and creating a stack

Fiji (https://fiji.sc)
SIFT plugin (https://imagej.net/Linear_Stack_Alignment_with_SIFT)

3.6 Segmenting out structures of interest

MIB (http://mib.helsinki.fi)

3.7 Rendering the segmented structures

Imaris

4 Results

The embedded sample of brain was imaged in the SBF-SEM with attention paid to the location of vessels within the field, and their proximity to others. Using SBF-SEM, sections of tissue were removed and single images captured to search the tissue block in the Z dimension. Initially five, 70 nm-slices were removed between images. When two or more vessels appeared which were converging, Z increments between imaging were decreased to single 70 nm slices. Fig. 1A shows two vessels of interest that were identified in the field (short arrows). As the sectioning continued (Fig. 1 B–D), the vessels began to converge and a branch point could be seen just under the block surface (Fig. 1D, arrowheads). As this sample had been previously imaged in the FIB-SEM the previous imaging area can also be seen in these micrographs (Fig. 1A, large arrowhead). At this point the sample was removed from the SBF-SEM and transferred to the FIB-SEM.

The ROI containing the possible convergent vessels was reacquired based on anatomical landmarks that could be visualized in the FIB-SEM by using 15 kV to image through the platinum layer (Fig. 2). Preparation of the sample for the FIB was carried out (Fig. 3 A–D) and a series of 2299, 5 nm slices was made with the Ga^+-ion beam

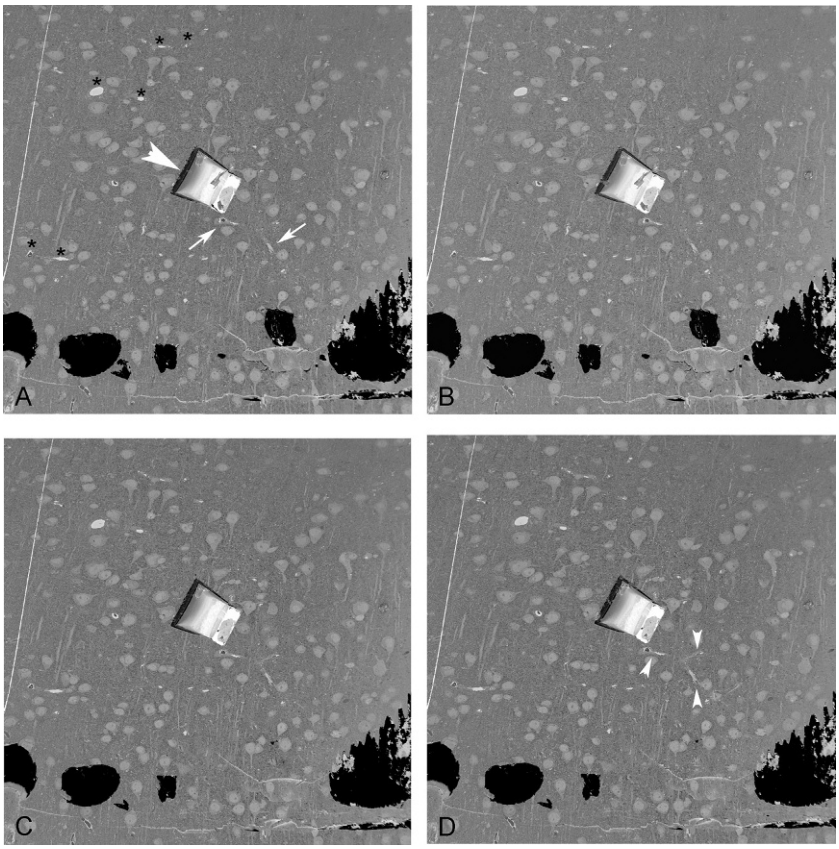

FIG. 1

Using the SBF-SEM to locate the structure of interest. (A) Initial view of the block surface indicating the presumptive converging vessel (arrows) and also containing a FIB-SEM trench from a previous run (arrowhead). The presumptive area of convergence is confirmed by successive removal of 350 nm (B), 140 nm (C) and 70 nm (D) of the surface until the area of interest is clearly seen (arrowheads). Black areas represent platinum remaining on the block surface.

(Supplemental Movie 1 in the online version at https://doi.org/10.1016/bs.mcb.2019.03.014). These images revealed the two vessels (Fig. 4A) that did associate with a pericyte cell body. The pericyte enveloped the two vessels and the processes continued throughout the run extending beyond the point where the imaging was stopped (Fig. 4 B–D). A partial reconstruction (Fig. 5) revealed the pericyte cell body and its ensheathing processes around the capillary (see also Supplemental Movie 2 in the online version at https://doi.org/10.1016/bs.mcb.2019.03.014).

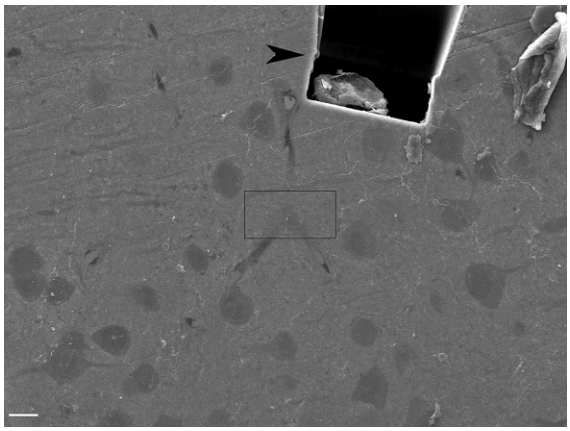

FIG. 2

The same area identified in the SBF-SEM imaged at 15 kV in the FIB-SEM to reveal the morphology underneath the surface. The area where the vessels appear to be convergent is identified with a box. The previous FIB-SEM trench acts as a good landmark. Scale bar = 10 μm.

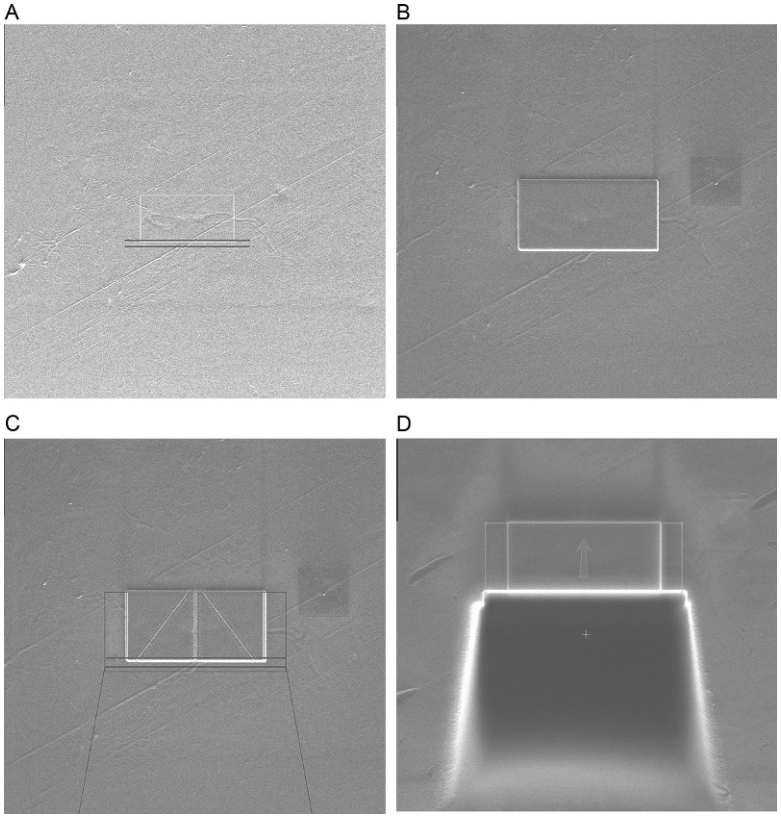

FIG. 3

Steps in the preparation of the block for imaging by FIB-SEM. (A) The vessel is seen using an image from the SEM and the area which will be imaged is selected (Box 3A). (B) A layer of platinum is applied using the FIB beam. (C) Marks for tracking and stigmation are applied using the FIB beam and Carbon deposition. (D) Material is removed to allow the electron beam to image the surface desired, the area which will be imaged is indicated by the box and the direction of sectioning by the arrow.

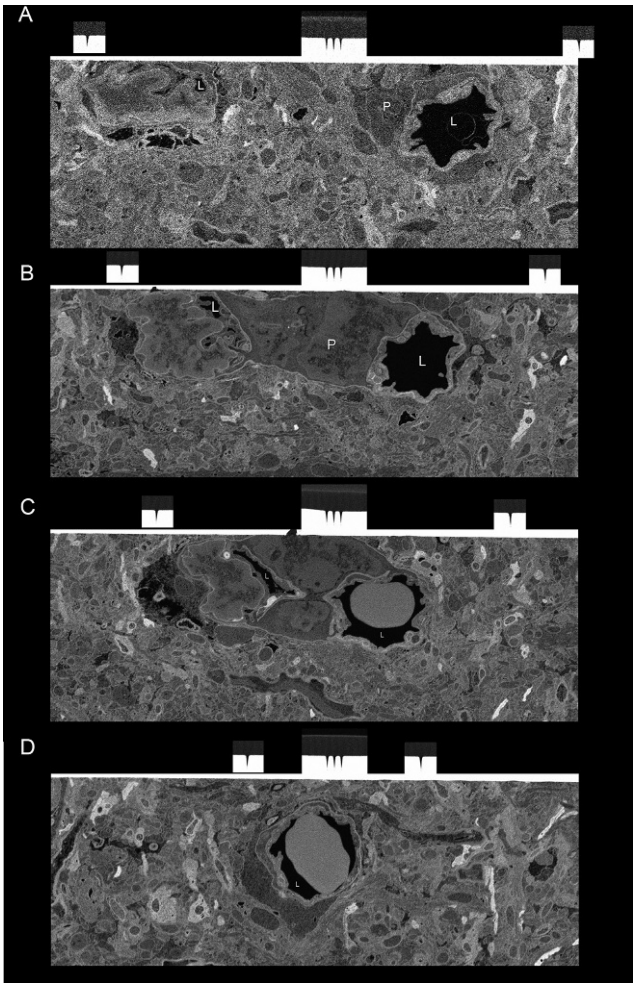

FIG. 4

Images from the FIB-SEM run. (A) First image in the run. Already the two vessel lumens are visible (L) as well as the pericyte cell body (P). The grainy nature of this image is due to the block face not yet being as smooth as it will be after additional milling. (B) Slice 500, the vessels are converging and the pericyte cell body fills the space between. (C) Slice 1000, the lumens are almost at the branch point. (D) Slice 2299, final slice in the run. The vessels are now merged and a blood cell nearly fills the luminal space. NB these images are as produced by the back scattered electron detector, their gray levels can be inverted if a more TEM-like image is desired.

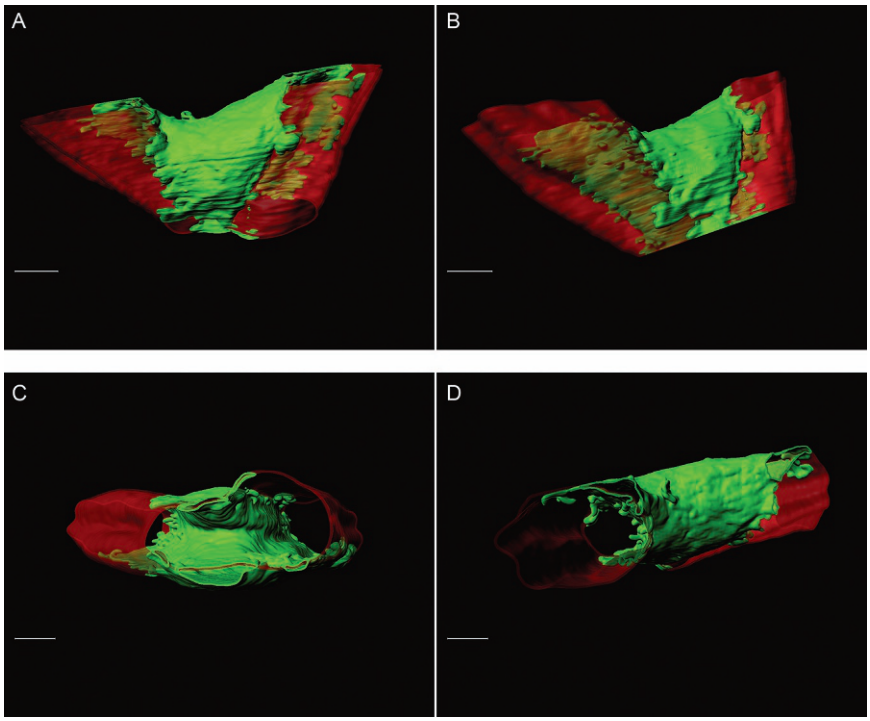

FIG. 5

Segmented reconstruction of the pericyte. Four views from the reconstructed pericyte (green) and blood vessel (red). (A) Top view showing the pericyte nestled in the junction where the vessel branches. (B) Slightly angled view showing more clearly the extent of pericyte envelopment of the vessel. (C) View from the junction up through the branching vessels. (D) View from the vessel junction end again showing the intricate association between pericyte and endothelium. All scale bars = 2 μm.

5 Discussion

Microscopy in the 21st century can handle samples of very different sizes and also produces images from macroscopic down to molecular resolution. This can produce a challenge when moving from one scale using one technique, to another with very different resolutions and field of view. Biological samples are frequently inhomogeneous and not every field of view will contain the information necessary to answer a given question. Therefore, the ability to search for a rare event in a larger volume is frequently necessary to find the structure of interest. The brain capillary network poses a unique challenge for ultrastructural imaging. Not only are individual capillary segments separated by tens of micrometers, the cells that comprise the vascular wall are intermittently spaced. The problem addressed here is how to locate and image a capillary associated pericyte in mouse brain. Pericytes have far reaching

processes that cover the majority of the capillary network. However, their cell bodies only contact 7% of the network (Underly et al., 2017), making them difficult to locate with 2D EM. Since pericyte somata occur frequently near capillary branch points, finding these regions increases the likelihood of capturing a pericyte soma. A detailed examination of pericyte substructure therefore requires electron microscopy and no single type of EM can provide an easy way to both find a pericyte and image it at high isotropic resolution in 3D.

This chapter describes a workflow in which two types of EM are combined to both identify the location and image a pericyte. SBF-SEM can make locating the probable location for a cell of interest relatively straightforward. It has been argued that using a very complex microscope such as a SBF-SEM just to find a particular ROI is an expensive solution to this problem, and that is correct. However, alternatives such as serial semi-thin (0.5 μm) sections may not be suitable if the structures of interest are smaller than that. Using serial TEM sections, which can be cut as thin as 70 nm, is very time consuming since it is necessary to cut, collect, stain and then image them before repeating the process for however many iterations required to locate the ROI. Using a SBF-SEM is far more efficient, and when the alternative is a more labor-intensive process using an equally expensive TEM, the actual savings at the end are debatable. In addition, the SBF-SEM technique is of sufficient resolution to answer many research questions on its own, so having access to this instrument as an additional, efficient screening platform is a bonus. In fact, both techniques have their strengths and their limitations and if possible placing both SBF-SEM and FIB-SEM in an imaging laboratory to use either independently, or in tandem as we show here, is tremendously cost-effective and powerful.

Although the sample preparation procedures for the two volume EM methods are similar, they are not identical, so when both techniques are used on the same sample some compromise is necessary. Staining must also take into account the specific tissue type and the structures that are to be identified and segmented out of the dataset after the imaging is finished (Kremer et al., 2015). In this example we employed a protocol that produced good contrast in the SBF-SEM but slightly overstained some structures such as myelin and lipid-rich lysosomes in the FIB-SEM. For volume EM using two different instruments with different detectors, optimization and sometimes some compromises are necessary to generate the most useful data set.

The segmentation of structures from volume EM datasets is not trivial, and as of now there are few computer algorithms that can process such datasets without some user input; though some semi-automated programs do exist (Sommer, Strähle, Köthe, & Hamprecht 2011). Advances in programming, processing speed and artificial intelligence algorithms will improve that situation but for this project manual segmentation using a digitizing tablet was the most efficient way to extract the structures of interest. Although the reconstruction here is only a partial pericyte, it is possible to obtain larger volumes and visualize greater tissue volumes.

The complexity of volume EM studies should not be underestimated. The equipment is expensive and cannot be run by non-experts. The procedures for fixation, staining, embedding, mounting, imaging and analyzing the data that comes from

such studies requires technical skills and experience. Yet, this technique, or in this case combination of techniques, is very informative. When a high-resolution image of a rare tissue event is needed to answer a scientific question, we believe the investment in equipment and personnel is well justified.

Acknowledgments

The authors would like to thank the VIB Core Facilities program, VIB Inflammation Research Center, Technology Fund and a generous Grant from minister Ingrid Lieten of the government of Flanders for support in implementing the SBF-SEM technology.

References

Belevich, I., Joensuu, M., Kumar, D., Vihinen, H., & Jokitalo, E. (2016). Microscopy image browser: A platform for segmentation and analysis of multidimensional datasets. *PLoS Biology, 14*(1). , e1002340. https://doi.org/10.1371/journal.pbio.1002340.

Daneman, R., Zhou, L., Kebede, A. A., & Arres, B. A. (2010). Pericytes are required for blood-brain barrier integrity during embryogenesis. *Nature*, *468*(7323), 562–566.

Darrow, M. C., Luengo, I., Basham, M., Spink, M. C., Irvine, S., French, A. P., et al. (2017). Volume segmentation and analysis of biological materials using SuRVoS (super region volume segmentation) workbench. *Journal of Visualized Experiments, 126*, e56162. https://doi.org/10.3791/56162.

Deerinck, T. J., Bushong, E. A., Thor, A., & Ellisman, M. H. (2010). NCMIR methods for 3D EM: A new protocol for preparation of biological specimens for serial block face scanning electron microscopy. *National Center for Microscopy and Imaging Research*. https://ncmir.ucsd.edu/sbem-protocol.

Denk, W., & Horstmann, H. (2004). Serial block-face scanning electron microscopy to reconstruct three dimensional tissue nanostructure. *PLoS Biology:11,* e329.

Hall, C. N., Reynell, C., Gesslein, B., Hamilton, N. B., Mishra, A., Sutherland, B. A., et al. (2014). Capillary pericytes regulate cerebral blood flow in health and disease. *Nature*, *508*(7494), 55–60.

Hartmann, D. A., Underly, R. G., Grant, R. I., Watson, A. N., lindner, V., & Shih, A. Y. (2015). Pericyte structure and distribution in the cerebral cortex revealed by high-resolution imaging of transgenic mice. *Neurophotonics, 2*(4), 041402.

Heymann, J. A., Hayles, M., Gestmann, I., Giannuzzi, L. A., Lich, B., & Subramaniam, S. (2006). Site specific 3D imaging of cells and tissues with a dual beam microscope. *Journal of Structural Biology*, *155*(1), 63–73.

Koster, A. J., Grimm, R., Hegerl, R., Stoschek, A., Walz, J., & Baumeister, W. (1997). Perspectives of molecular and cellular electron tomography. *Journal of Structural Biology*, *120*, 276–308.

Kremer, A., Lippens, S., Bartunkova, S., Asselbergh, B., Blanpain, C., Fendrych, M., et al. (2015). Developing 3D SEM in a broad biological context. *Journal of Microscopy*, *259*(2), 80–96.

Leighton, S. (1981). SEM images of block faces, cut by a miniature microtome within the SEM—A technical note. *Scanning Electron Microscopy*, 71–76 [pt 2].

Peddie, C. J., & Collinson, L. M. (2014). Exploring the third dimension: Volume electron microscopy comes of age. *Micron*, *61*, 9–19.

Sommer, C., Strähle, C., Köthe, U., & Hamprecht, F. A. (2011). Ilastik: Interactive learning and segmentation toolkit. In *Proceedings of Eighth IEEE International Symposium on Biomedical Imaging (ISBI)* (pp. 230–233).

Underly, R. G., Levy, M., Hartmann, D. A., Grant, R. I., Watson, A. N., & Shih, A. Y. (2017). Pericytes as inducers of rapid, matrix metalloproteinase-9-dependent capillary damage during ischemia. *The Journal of Neuroscience*, *37*(1), 129–140.

Yang, S., Jin, H., Zhu, Y., Wan, Y., Opoku, E. N., Zhu, L., et al. (2017). Diverse functions and mechanisms of pericytes in ischemic stroke. *Translational Stroke Research*, *8*(2), 107–121.